Active disturbance rejection control FCS-MPC strategy based on ESO of PMSM system

ZHANG Bin, WEN Xue, LI Kun-qi

(*School of Automation & Electrical Engineering, Lanzhou Jiaotong University, Lanzhou 730070, China*)

Abstract: In order to improve the control performance of three-phase permanent magnet synchronous motor (PMSM) system, an active disturbance rejection finite control set-mode predictive control (FCS-MPC) strategy based on improved extended state observer (ESO) is proposed in this paper. ESO is designed based on the arc-hyperbolic sine function to obtain estimations of rotating speed and back electromotive force (EMF) term of motor speed. Active disturbance rejection control (ADRC) is applied as speed controller. The proposed FCS-MPC strategy aims to reduce the electromagnetic torque ripple and the complexity and calculation of the algorithm. Compared with the FCS-MPC strategy based on PI controller, the constructed control strategy can guarantee the reliable and stable operation of PMSM system, and has good speed tracking, anti-interference ability and robustness.

Key words: extended state observer (ESO); auto disturbance rejection control (ADRC); finite control set-mode predictive control (FCS-MPC); permanent magnet synchronous motor (PMSM); arc-hyperbolic sine function

CLD number: TM341 **Document code**: A

Article ID: 1674-8042(2018)02-0140-08 **doi**: 10.3969/j.issn.1674-8042.2018.02.007

0 Introduction

Three-phase permanent magnet synchronous motor (PMSM) has many advantages such as simple structure, small volume, small moment of inertia and large power factor. So it has been widely used in important fields, such as transportation, military, industrial, medical and aviation[1,2]. The control methods of high performance PMSM system consist of vector control (VC)[3], direct torque control (DTC)[4,5] and model predictive control[6,7]. In recent years, a kind of optimization control method finite control set-mode predictive control (FCS-MPC) has been paid wide attention. FCS-MPC can be divided into current prediction control and torque prediction control[8,11] according to the control target[9,10,12].

In traditional torque prediction control, it is necessary to adjust the weight coefficient to ensure that the system has good dynamic performance, duing to the inconsistency between the stator flux and the electromagnetic torque[13]. In contrast, current prediction control has the same magnitude with the current variable, which can avoid to design weight coefficient. The traditional FCS-MPC needs to predict current values corresponding to all the basic voltage vectors in each sampling period, which makes it have heavy computing in the actual industrial control[14]. Zhang Y C[10] proposes a fast vector selection based on FCS-MPC, which reduces the complexity of computation and algorithm. As the back electromotive force (EMF) is DC amount, the method that estimates the back EMF of the current moment by calculating the values of the first three moments and averaging them will increase system complexity. Meanwhile, external interference will lead to estimation error. In this paper, the extended state observer (ESO) is applied to observe the back EMF in real time, and a new FCS-MPC strategy is constructed to improve the control performance of the system.

FCS-MPC speed control system of PMSM requires accurate rotational speed information. The speed sensor with higher accuracy and resolution is expensive, and there are problems such as complexity of the system, noise quantization and so on. Therefore, the study of speed sensorless has drawn

Received date: 2018-02-01

Foundation items: National Natural Science Foundation of China (No. 61461023); Gansu Provincial Department of Education Project (No. 2016B-036)

Corresponding author: WEN Xue (369605081@qq.com)

great attention. At present, the speed control methods of the motor system consist of high frequency injection (HFI)[15], extended kalman filter method (EKF)[16], model reference adaptive control (MRAS)[17], sliding mode (SM) variable structure[18] and extended state observer (ESO)[19]. The arc-hyperbolic sine function of many speed identification methods can make ESO have a good estimation effect, and the ESO based on the arc-hyperbolic sine function, which does not need accurate mathematical model, has strong anti-jamming capacity and rapid convergency and so on.

Speed regulator in FCS-MPC system of PMSM usually adopts PI algorithm. The control effect can be obtained by adjusting the PI parameters at different speeds and external disturbances. In order to improve the robustness of the system speed regulator, the authors proposed a new anti-disturbance rejection control strategy based on the arc-hyperbolic sine function[19-21] in recent years which has drawn wide concern. In the Ref. [20], the tracking differentiator of the arc-hyperbolic sine function is presented, in which the ideal differential signal can be obtained, and track response speed is quickly and stably. In Ref. [19], an extended state observer based on the arc-hyperbolic sine function is put forward. The observer can accurately observe the disturbance variable, and the response speed of the system is fast and stable. At the same time, the initial parameters of ESO can be used to suppress the differential amplitude. Active disturbance rejection control (ADRC), which does not require accurate mathematical models, has strong robustness and immunity. Therefore, ADRC based on arc-hyperbolic sine function is used as the speed regulator in this paper.

In order to improve the control precision, robustness and control performance of the system, the ADRC FCS-MPC strategy based on ESO is proposed for PMSM system, which can reduce the cost of sensor at the same time.

1 Mathematical model of PMSM

In this paper, taking the surface mounted PMSM system as the control object, that is $L_d=L_q=L$, so the mathematical model in the synchronous rotating reference frame is

$$\begin{cases}\dfrac{\mathrm{d}i_d}{\mathrm{d}t}=\dfrac{1}{L}(u_d-R_s i_d-e_d),\\ \dfrac{\mathrm{d}i_q}{\mathrm{d}t}=\dfrac{1}{L}(u_q-R_s i_q-e_q),\\ \dfrac{\mathrm{d}\omega_r}{\mathrm{d}t}=\dfrac{3P\psi_f}{2J}i_q-\dfrac{B}{J}\omega_r-\dfrac{T_L}{J},\\ \omega_e=P\omega_r,\end{cases}\tag{1}$$

where i_d, i_q and u_d, u_q are d, q axis currents and voltages of stators; R_s is stator resistor; L_s is stator inductance; e_d, e_q is back EMF; ω_r is rotor velocity; ω_e is electrical angular velocity; P is pole pairs; ψ_f is rotor permanent magnetic flux; T_L is load torque; J is moment of inertia; and B is coefficient of friction factor.

2 ADRC FCS-MPC strategy of PMSM system based on ESO

For the three-phase PMSM system, the system block diagram of active-disturbance rejection FCS-MPC based on ESO is shown in Fig. 1.

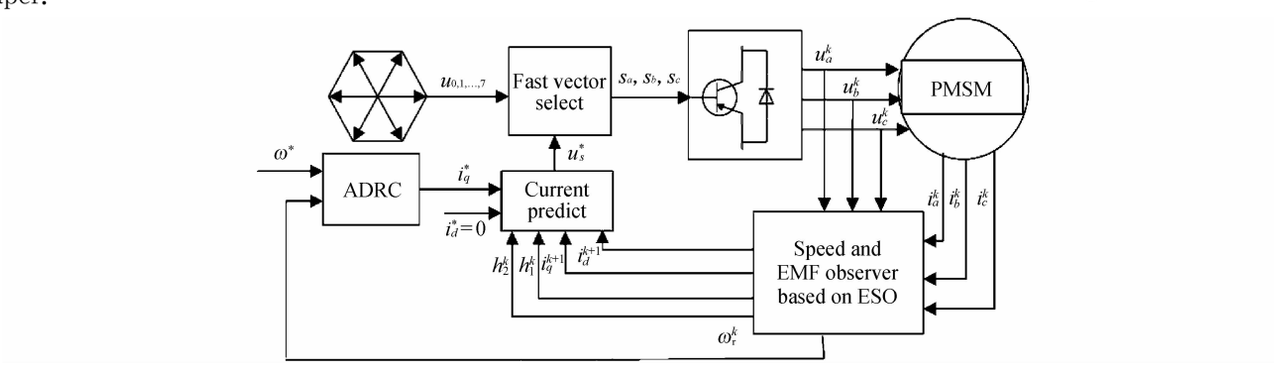

Fig. 1 System block diagram of active disturbance rejection FCS-MPC strategy based on ESO

2.1 Design of speed observer based on ESO

According to the principle of stator current state Eq. (1) of PMSM and ESO, the first order state space equation of the system is constructed as

$$\begin{cases}\dot{\boldsymbol{v}}_1 = -\dfrac{R_s}{L}\boldsymbol{v}_1 + \boldsymbol{h} + \dfrac{1}{L}\boldsymbol{u}, \\ \boldsymbol{y}_1 = \boldsymbol{v}_1, \end{cases} \tag{2}$$

where

$$\boldsymbol{v}_1 = [i_d \quad i_q],$$
$$\boldsymbol{u} = [u_d \quad u_q],$$
$$\boldsymbol{h} = [-e_d/L \quad -e_q/L],$$

And $\boldsymbol{h}$ in Eq. (2) is extended to the new state variable $\boldsymbol{v}_2$, where $\boldsymbol{q}$ is present, and $\boldsymbol{q}(t)$ is bounded. The extended equation of Eq. (2) is

$$\begin{cases}\dot{\boldsymbol{v}}_1(t) = -R_s\boldsymbol{v}_1(t)/L + \boldsymbol{v}_2(t) + \boldsymbol{u}(t)/L, \\ \dot{\boldsymbol{v}}_2(t) = \boldsymbol{q}(t), \\ \boldsymbol{y}(t) = \boldsymbol{v}_1(t). \end{cases} \tag{3}$$

Eq. (3) is observable, and the second-order ESO of Eq. (3) can be constructed as

$$\begin{cases}\boldsymbol{e}_1(t) = \boldsymbol{z}_1(t) - \boldsymbol{v}_1(t), \\ \dot{\boldsymbol{z}}_1(t) = -R_s\boldsymbol{z}_1(t)/L + \boldsymbol{z}_2(t) + \boldsymbol{u}(t)/L - \beta_1\boldsymbol{e}_1(t), \\ \dot{\boldsymbol{z}}_2(t) = -\beta_2\operatorname{arsh}(\beta_3\boldsymbol{e}_1(t)), \end{cases} \tag{4}$$

where $\beta_1>0$, $\beta_2>0$, $\beta_3>0$, and arsh(•) is a smooth continuous nonlinear function.

In the second-order ESO of Eq. (4), there are

$$\boldsymbol{z}_1 = [\hat{i}_d \quad \hat{i}_q]^{\mathrm{T}},\ \boldsymbol{z}_2 = [\hat{h}_1 \quad \hat{h}_2]^{\mathrm{T}},$$
$$\hat{h}_1 = -\hat{e}_d/L,\ \hat{h}_2 = -\hat{e}_q/L, \tag{5}$$

where $\hat{i}_d$, $\hat{i}_q$ are the estimated values of i_d, i_q; $\hat{h}_1$, $\hat{h}_2$ are the estimated values of counter electromotive items.

The observed value of ESO contains the information of speed, i. e. ,

$$\hat{h}_1 = \hat{\omega}_e\hat{\psi}_d/L,\ \hat{h}_2 = -\hat{\omega}_e\hat{\psi}_q/L,$$
$$\hat{\psi}_d = L\hat{i}_d + \psi_f,\ \hat{\psi}_q = L\hat{i}_q, \tag{6}$$

where $\hat{\psi}_d$, $\hat{\psi}_q$ are the estimated values of ψ_d, ψ_q. The estimated value ($\hat{\omega}_e$) and position ($\hat{\theta}_e$) can be obtained as

$$\hat{\omega}_e = \frac{\hat{\psi}_d L(\hat{h}_1 - \hat{h}_2)}{\hat{\psi}_d + \hat{\psi}_q},\ \hat{\theta}_e = \int\hat{\omega}_e\mathrm{d}t. \tag{7}$$

2.2 Design of active disturbance rejection speed regulator based on arc-hyperbolic sine function

ADRC consists of first-order tracking differentiator (TD), ESO and state error feedback control law. The speed tracking error can be reduced through the first step tracking differential. The system state and perturbation can be estimated by ESO in real time. The disturbance can be compensated by means of the state error feedback control law according to the separation principle. The structure is shown in Fig. 2.

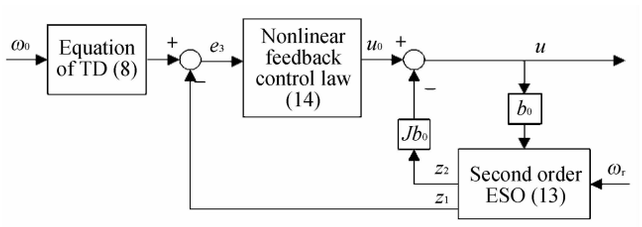

Fig. 2 Speed controller based on ADRC of PMSM system

2.2.1 Design of first order tracking differentiator

A differential equation of first order speed tracking is constructed by using arsh(•)[20] as

$$\begin{cases}e_1 = w - \omega_m, \\ \dot{w} = -b_1\operatorname{arsh}(a_1e_1), \end{cases} \tag{8}$$

where ω_m is speed setpoint value, w is the transition variable, parameters $b_1>0$, $a_1>0$. a_1 is close to 1 in usual. The appropriate increase of b_1 can increase the response speed and reduce the tracking error. The ideal response output of ω_m can be obtained by Eq. (8).

2.2.2 Design of second-order ESO

Let

$$x_1 = \omega_r,\ y_2 = x_1. \tag{9}$$

According to the speed differential equation constructed by Eq. (1), the first order state space equation is constructed as

$$\begin{cases}\dot{x}_1 = -Bx_1/J - T_L/J + b_0i_q, \\ y_2 = x_1, \end{cases} \tag{10}$$

where $b_0 = 1.5\psi_fP/J$, y_2 is the input of speed controller, i_q is the output of speed controller.

From Eq. (10), we can see that the load torque and viscous friction coefficient are changing interference signals. The various unknown disturbances are denoted by $f(t)$ as

$$f(t) = -B\omega_r/J - T_L/J. \tag{11}$$

Let $x_2(t)=f(x_1)$, and $x_2(t)$ is extended variable, that is $\dot{x}_2(t)=g(t)$. The first order system constructed by Eq. (10) is extended to

$$\begin{cases}\dot{x}_1(t) = x_2(t) + b_0 i_q(t), \\ \dot{x}_2(t) = g(t), \\ y(t) = x_1(t). \end{cases} \tag{12}$$

The second-order extended state observer of the structural system constructed by Eq. (12) is

$$\begin{cases} e_2(t) = z_1(t) - y(t), \\ \dot{z}_1(t) = z_2(t) - b_2 e_2(t), \\ z_2(t) = -b_3 \mathrm{arsh}(a_2 e_2(t)), \end{cases} \tag{13}$$

where $b_2>0$, $b_3>0$, $a_2>0$. a_2 is close to 1 in usual. The astringency of ESO is easy to be influenced by parameter b_2. The extended state observer constructed by Eq. (13) can achieve accurate state variable estimation of the expansion Eq. (12) only when $b_2 - b_3 a_2 > 0$, that is $z_1(t) \to x_1(t)$, $z_2(t) \to x_2(t)$.

2.2.3 First-order active-disturbance rejection controller

The error feedback control rate $u_0(t)$ shown in Fig. 2 is used to feed forward the interference signal. It is designed as

$$\begin{cases} e_3 = w - z_1, \\ u_0 = b_4 \mathrm{arsh}(a_3 e_3), \\ u = u_0 - z_2 / b_0, \end{cases} \tag{14}$$

where parameters $b_4>0$, $a_3>0$. a_3 is close to 1 in usual. A small ripple of control quantity u can be got by selecting the proper value of b_4.

2.3 FCS-MPC based on fast vector selection

According to Eqs. (1) and (6), the current space state vector differential equation under the selected rotation coordinate axis is constructed as

$$\boldsymbol{i}_s = (\boldsymbol{u}_s - R_s \boldsymbol{i}_s)/L_s - \boldsymbol{z}_2, \tag{15}$$

where $\boldsymbol{i}_s = [i_d \quad i_q]$ is current vector; $\boldsymbol{u}_s = [u_d \quad u_q]$ is voltage vector.

2.3.1 Current model predictive control based on fast vector selection

The traditional FCS-MPC calculates the predicted current for each fundamental voltage vector in the rotating coordinate system first, and then calculates the corresponding minimum objective function value based on the predicted current, finally selects the voltage vector of the minimum objective function as the best output of the inverter. But it needs to forecast current for 7 times, which makes the amount of calculation relatively large. In order to obtain better control effect, the FCS-MPC strategy based on fast vector selection is presented in Ref. [10], in which the optimal voltage vector is obtained fast by summing the average to estimate the back EMF. Therefore, complexity of the algorithm and the computation is obviously reduced. However, the estimation of back EMF will increase the complexity of the computation and system, and external interference will lead to estimation error. In this paper, the Eq. (5) is used to estimate the back EMF.

In this paper, the second-order Eulerian discretization method is applied to further simplify the Eq. (10)[10], that is

$$\boldsymbol{i}_s^{k+1} = \boldsymbol{i}_{s0}^k + \frac{T_s L_s - 0.5 T_s^2 R_s}{L^2} \boldsymbol{u}_s^k, \tag{16}$$

where

$$\boldsymbol{i}_{s0}^k = \frac{(L_s^2 - L R_s T_s + 0.5 T_s^2 R_s^2)\boldsymbol{i}_s^k - 0.5 T_s^2 R_s \boldsymbol{z}_2^k}{L}.$$

In Eq. (16), the ideal voltage vector is obtained when $\boldsymbol{i}_s^{k+1} = \boldsymbol{i}_s^*$, i.e.,

$$\boldsymbol{u}_s^* = \frac{L_s^2 (\boldsymbol{i}_s^* - \boldsymbol{i}_{s0}^k)}{T_s L - 0.5 T_s^2 R_s}. \tag{17}$$

Let $\boldsymbol{u}_k$ ($k = 1, 2, \cdots, 6$) be the the base voltage vector of 6 sectors, and as long as the amplitude of the error vector is the smallest, i.e.,

$$\boldsymbol{e}_{uk} = | \boldsymbol{u}_s^* - \boldsymbol{u}_k |. \tag{18}$$

When the output basic voltage vector is zero vector, the amplitude of the error vector is

$$\boldsymbol{e}_0 = | \boldsymbol{u}_s^* |. \tag{19}$$

The method can be summarized as follows: (1) $\boldsymbol{u}_s^*$ is calculated by Eq. (17). (2) Judging the sector k ($k=1, 2, \cdots, 6$) that $\boldsymbol{u}_s^*$ located by Eq. (18). (3) Comparing $\boldsymbol{e}_0$ with $\boldsymbol{e}_{uk}$ by Eqs. (18) and (19). If $\boldsymbol{e}_0 > \boldsymbol{e}_{uk}$, the best voltage vector is $\boldsymbol{e}_{uk}$, otherwise, the best voltage vector is $\boldsymbol{e}_0$.

2.3.2 Control of delay compensation

The actual output voltage of the controller lags the current change in the actual digital system control[22]. To eliminate the negative effect of the system control performance by the delay, $\boldsymbol{i}_s^{k+1}$ is calculated according to Eq. (36) in Ref. [14], and then the voltage $\boldsymbol{u}_s^*$ is compensated at $k+1$ by appling the second-order Euler discretization method, which compensates the delay of the system.

$$\boldsymbol{i}_s^{k+1} = \boldsymbol{i}_{sp}^{k+1} - \frac{0.5 T_s R_s (\boldsymbol{i}_{sp}^{k+1} - \boldsymbol{i}_s^k)}{L_s}, \tag{20}$$

where $\boldsymbol{i}_{sp}^{k+1}=\boldsymbol{i}_{s}^{k}+\boldsymbol{z}_{2}^{k}+\dfrac{T_s(\boldsymbol{u}_{s}^{k}-R_s\boldsymbol{i}_{s}^{k})}{L_s}$.

The flow diagram of FCS-MPC based on fast vector selection is shown in Fig. 3 with considering the delay compensation.

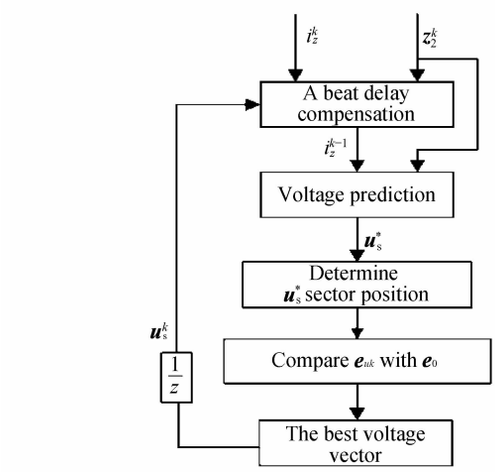

Fig. 3 FCS-MPC flow chart based on fast vector selection

3 Simulation analysis

The model of Fig. 1 is structured and simulated in Matlab/Simulink environment. The simulation parameters of PMSM system are shown in Table 1. The sampling period of the system is 10 μs. In order to verify the correctness and validity of the active-disturbing FCS-MPC method of PMSM system based on ESO, two FCS-MPC systems based on PI and ADRC are constructed by appling the same speed ESO parameters, and they are compared and analyzed.

Table 1 Parameters of PMSM

Parameter	Symbol	Data
Stator resistance	$R_s(\Omega)$	3.45
Winding inductance	L_s(H)	0.012
Rated power	P_N(kW)	1.1
Friction coefficient	B_m	0.05
Pole pair	P	2
Moment of inertia	J (kg·m^2)	0.001 54
Rated torque	T_N(N·m)	3
DC power supply	U_{dc}(V)	380
Rated speed	ω_N(r/min)	1 000

3.1 Comparison of anti-load ability

Adjusting PI parameters to obtain the same transient of the two systems so that they can meet the rationality comparison. When simulation, the speed setpoint of PMSM system is 1 000 r/min, the PMSM system starts with load (1 N·m) and is loaded to the rated load (3 N·m) at 0.2 s. The response curves of two systems are shown in Figs. 4 and 5, respectively.

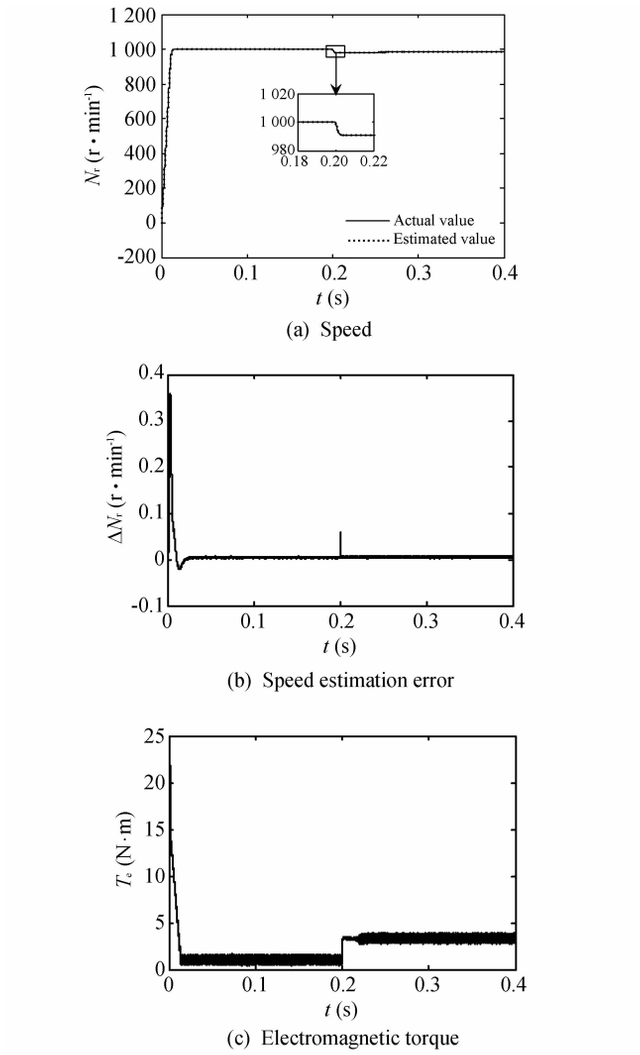

Fig. 4 Dynamic response of speed sensorless PMSM system based on PI FCS-MPC strategy

Simulation analyses are as follows.

1) ESO speed estimation. As can be seen from Figs. 4 and 5(a) and (b), both the FCS-MPC PMSM systems based on PI and ADRC, the ESO speed estimates and the actual curves are almost coincident, and the speed errors are small, i.e., the speed observer can be quickly tracked and has a high recognition accuracy.

2) Robustness of ative-disturbance FCS-MPC strategy for three-phase PMSM. Figs. 4 and 5(a) show that the FCS-MPC PMSM system based on ADRC has smaller torque ripple and can be restored to the reference value, which means that it has a stronger anti-load capacity comparing with the FCS-MPC PMSM system based on PI. As can be seen from Figs. 4 and 5(c), the FCS-MPC PMSM system

based on PI has the smaller electromagnetic torque ripple compared to the FCS-MPC PMSM system based on ADRC.

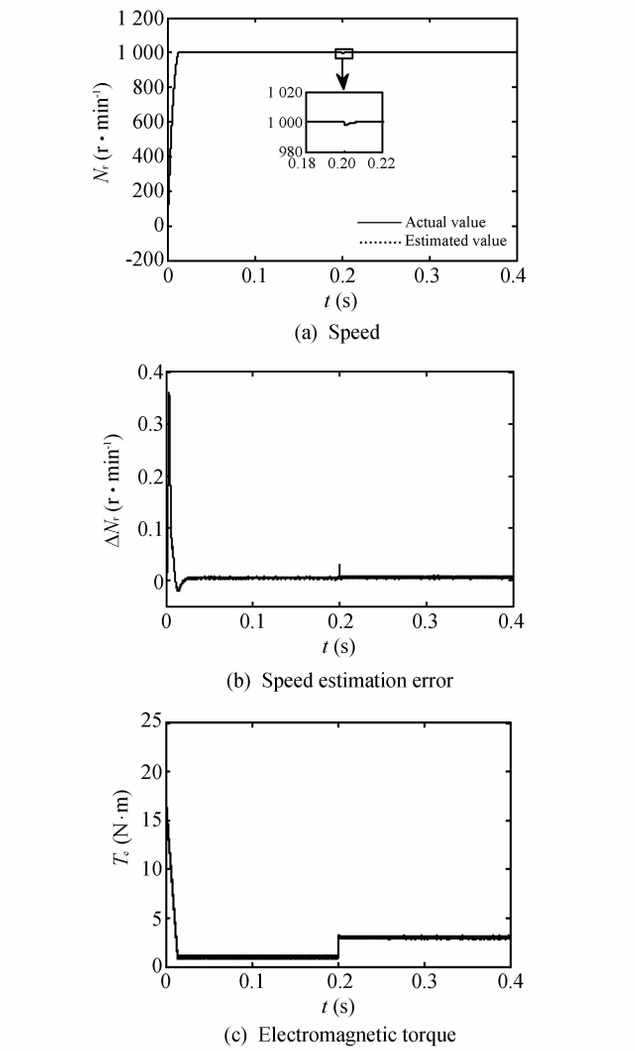

Fig. 5 Dynamic response of PMSM system based on ADRC with FCS-MPC strategy

3.2 Comparison of transient response characteristics

PI parameters are adjusted so that two FCS-MPC PMSM systems based on PI and ADRC have the same anti-load change capability as possible for which can meet the rationality comparison. When simulation, the speed setpoint of PMSM system is 1 000 r/min, the PMSM system start with load (1 N·m) and is loaded to the rated load (3 N·m) at 0.2 s. The response curves of two systems are shown in Figs. 6 and 7, respectively.

The following results can be obtained by simulation analysis.

1) ESO speed estimation. As can be seen from Figs. 6 and 7(a) and (b), both the FCS-MPC PMSM systems based on PI and ADRC, the ESO speed estimates and the actual curves are almost coincident, and the speed errors are small, that is, the speed observer can be quickly tracked and has a high recognition accuracy.

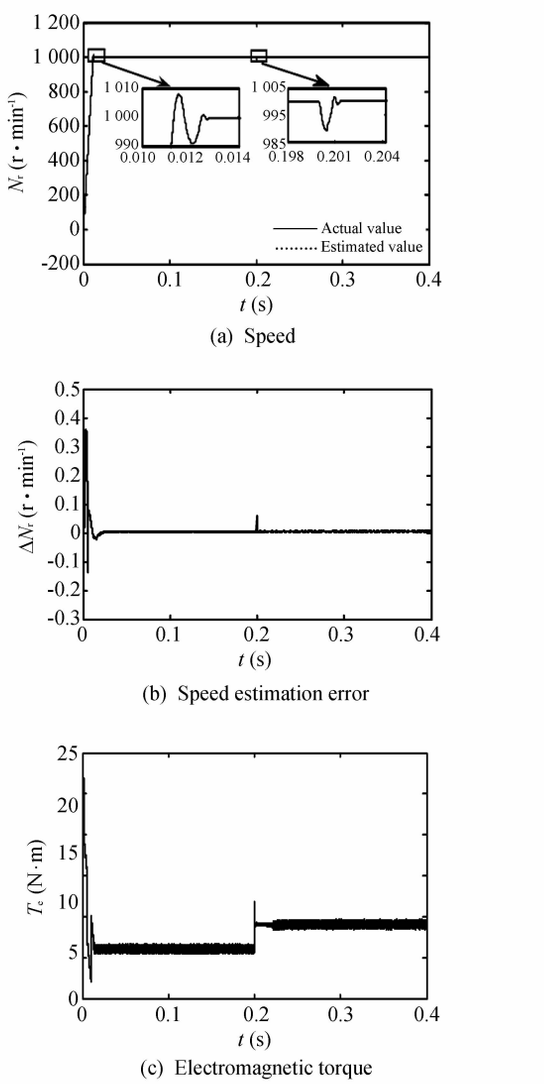

Fig. 6 Dynamic response of FCS-MPC strategy on speed sensorless PMSM system based on PI

2) Robustness of active-disturbance FCS-MPC strategy for three-phase PMSM. From Figs. 6 and 7(a), the FCS-MPC PMSM system based on ADRC has smaller overshoot and shorter control period when the resistance to load change is consistent, and it has better speed transient response characteristics. As can be seen from Figs. 6 and 7(c), the FCS-MPC PMSM system based on PI has the smaller electromagnetic torque ripple compared to the FCS-MPC PMSM system based on ADRC.

Above all, the control method designed in this paper can guarantee the stable operation of the system when the load changes, and it can ensure the

system has strong anti-load interference ability, low electromagnetic torque ripple, and good dynamic performance. It does better than PI control in the anti-load capacity and dynamic performance.

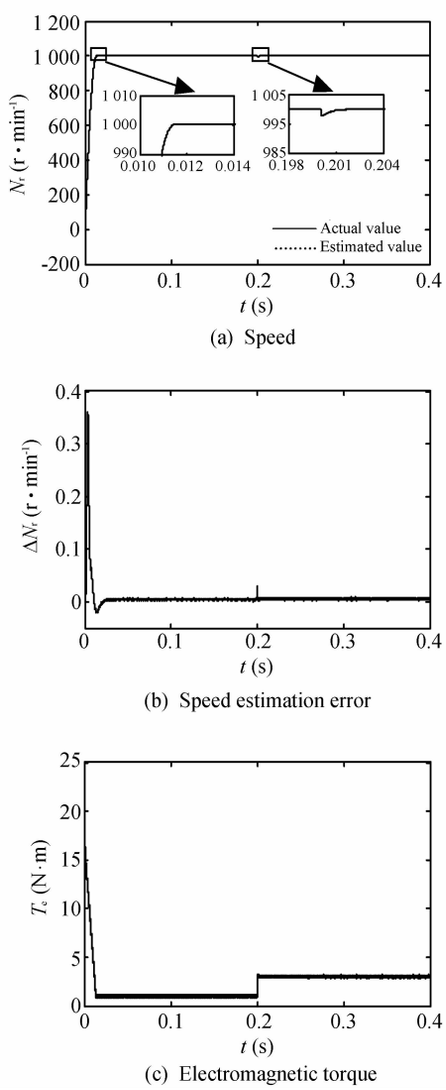

Fig. 7 Dynamic response of FCS-MPC strategy of speed sensorless PMSM system based on ADRC

4 Conclusion

In this paper, an active-disturbance-rejection FCS-MPC strategy based on ESO speed sensorless of surface mounted PMSM was proposed. ESO based on arsh(•) is designed to estimate the speed and back EMF term accurately. Compared with the PI-based FCS-MPC system, it can ensure that the system has strong anti-load interference ability, small electromagnetic torque ripple and good dynamic performance, which can achieve satisfactory torque and speed control effect. Actual results indicate the correctness and feasibility of the proposed method.

References

[1] Dai Y, Song L, Cui S. Development of PMSM drives for hybrid electric car applications. IEEE Car Transactionson Magnetics, 2007, 43(1): 434-437.

[2] Xia C L, Yan Y. Matrix converter permanentmagnet synchronous motor drives. Transactionof China Eletrotechnical Society, 2015, 30(23): 1-9.

[3] Rashed M, Macconnell P F A, Stroncach A, et al. Sensorless indirect rotor field orientation speed control of permanent magnet synchronous motor using adaptive rotor flux estimator. In: Proceedings of the 44th IEEE Conference on Decision and Control, 2005.

[4] Simanek J, Novak J, Cerny O, et al. FOC and flux weakening for traction drive with permanent magnet synchronous motor. In: Proceedings of IEEE International Symposium on Industrial Electronics. IEEE Xplore, 2008: 753-758.

[5] Foo G, Sayeef S, Rahman M F. Low-speed and standstill operation of a sensorless direct torque and flux controlled IPM synchronous motor drive. IEEE Transactions on Energy Conversion, 2010, 25(1): 25-33.

[6] Rodriguez J, Cortes P. Predictive control of power converters and electrical drives. Predictive Control of Power Converters & Electrical Drives, 2012, 6(4): 1785-1786.

[7] Moon H T, Kim H S, Youn M J. A discrete-time predictive current control for PMSM. IEEE Transactions on Power Electronics, 2003, 18(1): 464-472.

[8] Geyer T, Papafotiou G, Morari M. Model predictive direct torque control—Part I: concept, algorithm, and analysis. IEEE Transactions on Industrial Electronics, 2009, 56(6): 1894-1905.

[9] Preindl M, Schaltz E. Sensorless model predictive direct current control using novel second-order pllobserver for pmsm drive systems. Industrial Electronics IEEE Transactions on, 2011, 58(9): 4087-4095.

[10] Zhang Y C, Yang H T, Wei X L. Prediction control of permanent magnet synchronous motor model based on fast vector selection. Journal of Electrical Engineering, 2016, 31(6): 66-73.

[11] Rodriguez J, Kennel R M, Espinoza J R, et al. High performance control strategies for electrical drives: an experimental assessment. IEEE Transactions on Industrial Electronics, 2012, 59(5): 812-820.

[12] Morel F, Lin S X, Retif J M, et al. A comparative study of predictive current control schemes for a permanent magnet synchronous machine drive. IEEE Transactions on Industrial Electronics, 2009, 56(7): 2715-2728.

[13] Cortes P, Kouro S, La Rocca B, et al. Guidelines forweighting factors design in Model Predictive Control of power converters and drives. IEEE International Conference on Industrial Technology, 2009: 1-7.

[14] Zhang Y C, Gao S Y. Measurement and prediction ofpermanent magnet synchronous motor considering delay compensation. Journal of Electrical Engineering, 2016,

11(3): 13-20.
[15] Zhu Z Q, Gong L M. Investigation of effectiveness of sensorless operation in carrier signal-injection-based sensorless controlmethod-s. IEEE Transactions on Industrial Electronics, 2011, 58(8): 3431-3439.
[16] Smidl V, Peroutka Z. Reduced-order square-root EKF for sensorless control of PMSM drives. Conference of the IEEE Industrial Electronics Society, 2011, 6854(5): 2000-2005.
[17] Orlowska K T, Dybkowski M. Stator-current-based mras estimator for a wide range speed sensorless induction-motor drive. IEEE Transactions on Industrial Electronics, 2010, 57(4): 1296-1308.
[18] Teng Q F, Bai J Y, Zhu J G, et al. Predictive torque control of three phase permanent magnet synchronous motor based on sliding mode modelreference adaptive observer. Control Theory & Applications, 2015, 32(2): 150-161.
[19] Zhou T. Expansive state observer based on inverse hyperbolic sine function. Control and Decision, 2015, 30(5): 943-946.
[20] Zhao T. Study on tracking differentials based on inverse hyperbolic sine function. Control and Decision, 2014, 29(6): 1139-1142.
[21] Zhao L Y, Wang S J. Automatic disturbance control based on arctangent nonlinear function. Journal of Shanghai Jiaotong University, 2013, 47(7): 1043-1048.
[22] Miranda H, Cortes P, Yuz J I, et al. Predictive torque control of induction machines based on state space models. IEEE Transactions on Industrial Electronics, 2009, 56(6): 1916-1924.

基于 ESO 的 PMSM 系统自抗扰 FCS-MPC 策略

张 斌，汶雪，李坤奇

（兰州交通大学 自动化与电气工程学院，甘肃 兰州 730070）

摘 要： 为了提高三相永磁同步电机(PMSM)系统的控制性能，以反双曲正弦函数为基础，通过改进的扩张状态观测器(ESO)获取转速和反电动势项高精度估值，以自抗扰控制作为转速控制调节器，提出了基于 ESO 的自抗扰有限控制集模型预测控制(FCS-MPC)策略，以减小电磁转矩脉动，降低算法的复杂性和计算量。与基于 PI 的 FCS-MPC 策略相比，新的控制策略能够保证 PMSM 系统稳定运行，具有良好的转速跟踪性、抗干扰性和鲁棒性。

关键词： 扩张状态观测器；自抗扰控制；有限状态模型预测控制；永磁同步电机；反双曲正弦函数

引用格式： ZHANG Bin, WEN Xue, LI Kun-qi. Active disturbance rejection control FCS-MPC strategy based on ESO of PMSM system. Journal of Measurement Science and Instrumentation, 2018, 9(2): 140-147. [doi: 10.3969/j.issn.1674-8042.2018.02.007]